# Structure and Photocatalytic Activity of $Ti_{1-x}M_xO_{2\pm\delta}$ (M = W, V, Ce, Zr, Fe, and Cu) Synthesized by Solution Combustion Method

**K. Nagaveni,[†] M. S. Hegde,[†] and Giridhar Madras*[,‡]**

*Solid State and Structural Chemistry Unit, Indian Institute of Science, Bangalore-560012, India, and Department of Chemical Engineering, Indian Institute of Science, Bangalore-560012, India*

*Received: May 15, 2004; In Final Form: August 12, 2004*

The W, V, Ce, Zr, Fe, and Cu metal ion substituted nanocrystalline anatase $TiO_2$ was prepared by solution combustion method and characterized by XRD, Raman, BET, EPR, XPS, IR TGA, UV absorption, and photoluminescence measurements. The structural studies indicate that the solid solution formation was limited to a narrow range of concentrations of the dopant ions. The photocatalytic degradation of 4-nitrophenol under UV and solar exposure was investigated with $Ti_{1-x}M_xO_{2\pm\delta}$. The degradation rates of 4-nitrophenol with these catalysts were lesser than the degradation rates of 4-nitrophenol with undoped $TiO_2$ both with UV exposure and solar radiation. However, the photocatalytic activities of most metal ion doped $TiO_2$ are higher than the activity of the commercial $TiO_2$, Degussa P25. The decrease in photocatalytic activity is correlated with decrease in photoluminescence due to electron states of metal ions within the band gap of $TiO_2$.

## Introduction

$TiO_2$, mainly in the anatase phase, has been employed for the degradation of several environmental contaminants under UV.[1−4] Several attempts have been made to improve the performance of $TiO_2$ as a photocatalyst under UV illumination and to extend its absorption and conversion capacity into the visible portion of the solar spectrum. Asahi et al.[5] reported that doping of $TiO_2$ by nitrogen, to $TiO_{2-x}N_x$, shifts its optical absorption into the visible region of $\lambda < 500$ nm. A similar study was reported by Khan et al.[6] on a chemically modified, carbon substituted $TiO_2$ absorbing light at wavelengths below 535 nm. Recently, a carbon doped titania, $TiO_{2-2x}C_xV^-_{O^{2-}}$ by solution combustion method, was synthesized that had an optical absorption below 600 nm and enhanced solar photocatalytic activity[7] compared to commercial Degussa P25. Hence, doping of anionic species such as C, N, F, or S for O (2p) seems to be effective in reducing the band gap and enhancing the photoactivity of $TiO_2$.

The influence of various transition metal ions on the photoactivity of pure $TiO_2$ for many reactions has also been studied with the aim of improving the efficiency of the photocatalytic process.[9−19] It has been hypothesized that the addition of transition metals to titania increases the rate of photocatalytic oxidation, due to the electron scavenging by the metal ions at the semiconductor surface through the following reaction: $M^{n+} + e^-_{CB} \rightarrow M^{(n-1)+}$, where $M^{n+}$ represents transition metal ions.[8] This reaction prevents electron−hole recombination and results in an increased rate of formation of $^{\bullet}OH$ radical.

Even though metal ion doping effects on the reactivity of $TiO_2$ have been extensively studied, there is a considerable controversy.[8−21] Some investigators report that doping of ions such as $V^{5+}$, $Cu^{2+}$, $Fe^{3+}$, and $W^{6+}$ in $TiO_2$ increases its photoactivity, whereas others have shown that doping can reduce the photoactivity. Reasons for lower or higher activity compared to pure $TiO_2$ are not yet clear.

Most of these metal doped $TiO_2$'s reported in the literature are prepared by coprecipitation and incipient wet impregnation method. In the impregnation method, substitution of metal ions in the bulk $TiO_2$ crystallites is not likely to occur, and at best, substitution may take place on the surfaces.[9,14] In the coprecipitation method, postheat processing of mixed metal hydroxides yields metal doped $TiO_2$. This high temperature, long time heating may separate out the dopant metal ions into respective metal oxides and in many cases they segregate on the surfaces.[18] Therefore, preparation of $Ti_{1-x}M_xO_{2\pm\delta}$ (M= transition metal ions) in anatase phase is critical to assess the effect of metal ion doping toward photocatalysis.

The solution combustion method is a novel technique in producing metal substituted oxides.[22−24] Unlike traditional methods, in the combustion synthesis, a temperature up to 700−800 °C is reached for a few seconds and the material is quenched to 300 °C quickly. Since this method is a solution process, it has all the advantages of wet chemical processes such as control of stoichiometry, doping of desired amount of transition metal ions. The present work was aimed at producing metal ion substituted $TiO_2$ by the solution combustion method and studying the influence of substitution on structure, extent of substitution and performance as a photocatalyst. The metal ions chosen for doping are lower valent ($Cu^{2+}$, $Fe^{3+}$), isovalent ($Ce^{4+}$, $Zr^{4+}$), and higher valent ($W^{6+}$, $V^{5+}$) ions. The photodegradation of 4-nitrophenol in aqueous suspension was used as a probe reaction to evaluate the photoactivity of the metal doped $TiO_2$.

## Experimental Section

**Synthesis of the Catalyst.** The $TiO_2$ employed in the present study was prepared by the solution combustion method. In a typical combustion synthesis, a Pyrex dish (300 $cm^3$) containing an aqueous redox mixture of titanyl nitrate (2g) and glycine (0.8878 g) in 15 mL of water was introduced into the muffle

[†] Solid State and Structural Chemistry Unit.
[‡] Department of Chemical Engineering.
* To whom correspondence should be addressed. E-mail: giridhar@chemeng.iisc.ernet.in. Fax: +91-80-360-0683.

10.1021/jp047917v CCC: $27.50 
Published on Web 11/25/2004

furnace preheated to 350 °C. The solution undergoes dehydration and a spark appears at one corner, which spreads throughout the mass yielding a voluminous solid product.[25−27]

Metal substituted $TiO_2$ was prepared by the solution combustion method by taking precursors $ZrO(NO_3)_2 \cdot H_2O$, $(NH_4)_2Ce(NO_3)_6$, $NH_4VO_3$, $H_2WO_4$, $Cu(CO_3)Cu(OH)_2$, and $Fe(NO_3)_3 \cdot 9H_2O$. The dopant concentrations varied between 1 and 10 atom %. The combustion mixture for the preparation of 5 atom % $Fe/TiO_2$ contained titanyl nitrate, ferric nitrate, and glycine in the mole ratio 0.95:0.05:1.14. Metal doped $TiO_2$ samples displayed various colors depending on the kind of metal ions used: Ce and Zr doped samples were dark yellow, Cu doped samples were green in color, V and Fe doped samples were brownish, and W doped $TiO_2$'s were pale yellow in color.

**Characterization of the Combustion Product.** X-ray diffraction (XRD) patterns of the powders were recorded with Siemens D5005 diffractometer with Cu Kα radiation ($\lambda$ = 1.5418 Å) at a scan rate of 1°/min. Rietveld profile fitting has been carried out to show the metal ion substitution for $Ti^{4+}$ sites. Crystallite size was determined using the Scherrer equation

$$L = \frac{(0.9\lambda 180)}{(\pi \mathrm{FWHM}_{hkl} \cos\theta)}$$

where $FWHM_{hkl}$ is the full width at half-maximum of an *hkl* peak at $\theta$ value. The Brunauer−Emmett−Teller (BET) surface area was determined using standard BET apparatus (NOVA-1000, Quantachrome, USA). The crystal structure was further analyzed by Raman spectroscopy (Bruker RFS 100/S). EPR spectra of pure and metal doped $TiO_2$ were obtained using Bruker ER 2000D spectrometer operating in the X-band (frequency ∼ 9.43 GHz). The as-synthesized catalyst was subjected to gravimetric-differential thermal analysis (TG-DTA) (Perkin-Elmer- Pyris Diamond) to determine the adsorbed water. FTIR studies were carried out in the 400−4000 $cm^{-1}$ frequency range in the transmission mode (Perkin-Elmer, USA, FTIR−Spectrum-1000). X-ray photoelectron spectroscopy (XPS) of these materials was recorded on an ESCA-3 Mark II spectrometer (VG Scientific Ltd. England) using Al Kα radiation (1486.6 eV). UV−vis absorption spectra of $TiO_2$ powders were obtained for the dry pressed disk samples using a UV−vis spectrophotometer (GBC Cintra 40, Australia) between 270 and 800 nm range and absorption spectra were referenced to $BaSO_4$. Each sample was dry-pressed into a 10-mm diameter round disk containing about 150 mg. The photoluminescence measurements were performed on a luminescence spectrometer (Perkin-Elmer LS 55) at room temperature under the excitation light of 285 nm. The conditions are fixed as far as possible in order to compare the photoluminescence signals directly.

**Photocatalytic Evaluation.** All of the experiments were carried out using a cylindrical annular batch photoreactor. The design and operation of the reactor have been discussed in detail elsewhere.[25] A medium pressure mercury vapor (MPML) lamp of 125 W (Mysore Lamps, India) was placed inside the reactor after carefully removing the outer shell. The lamp radiated predominantly at 365 nm (3.4 eV). All the solar experiments were carried out in a cylindrical borosilicate glass reactor with i.d., of 8 cm and 400 $cm^3$ volume. Direct sunlight was used in the present study, and the average solar intensity was 0.753 kW/$m^2$. Samples were collected at regular intervals for subsequent analysis by a UV−vis spectrophotometer (Shimadzu, UV-2100). 4-Nitrophenol was selected as a model pollutant for the photocatalytic degradation experiments because it is nonvolatile and a common contaminant in industrial wastewater. All degradations were performed in an open system wherein the top surface of the photoreactor was open to air providing enough oxygen for the oxidative degradation of pollutants. The reaction was carried out at 25 °C, maintained by circulating water in the annulus of the reactor and samples were collected at regular intervals for subsequent analysis by a UV−vis spectrophotometer (Shimadzu, UV-2100). For degradation experiments, 1 kg/$m^3$ of the catalyst and 0.5 mM 4-nitrophenol was selected as it gives the highest degradation rate using combustion synthesized $TiO_2$.[27]

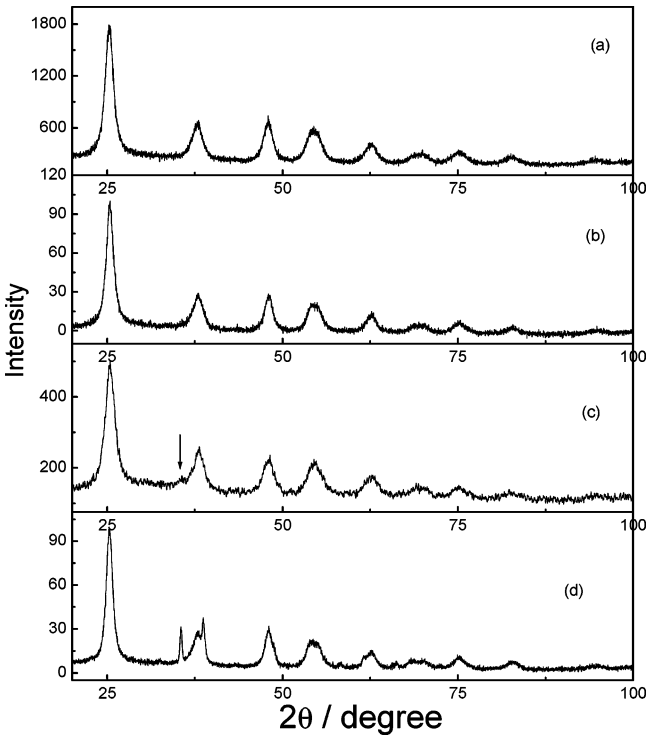


**Figure 1.** X-ray diffraction pattern of (a) combustion synthesized $TiO_2$, (b) 7.5 atom % $Cu/TiO_2$, (c) 10 atom % $Cu/TiO_2$, (d) physical mixture of 7.5% CuO + $TiO_2$.

## Results

**XRD Studies.** *$Ti_{1-x}Cu_xO_{2-\delta}$*. XRD patterns of pure $TiO_2$ and Cu ion substituted titania are shown in Figure 1. The pattern can be indexed to the $TiO_2$ anatase phase only, and no rutile or brookite impurities are detected. Cu doped titania does not show measurable CuO diffraction peaks up to 7.5 atom % and CuO lines are observed at 10 atom % $Cu/TiO_2$. To examine the expected CuO peak intensity in the XRD pattern, CuO nanoparticles prepared by the combustion method were physically mixed with pure anatase $TiO_2$ to 7.5 atom % CuO. The XRD pattern of the physical mixture shows intense peaks due to CuO along with anatase $TiO_2$ [Figure 1d].

Rietveld refinement of slow scanned (0.3°/min) data of 7.5 atom % $Cu/TiO_2$ was carried out by varying 16 parameters such as overall scale factor, background parameters, unit cell, shape and isotropic thermal parameters, and oxygen occupancy using the Fullprof-98 program. Rietveld is a least-square fit method, where the difference between the observed and the calculated parameters from the proposed model is minimized. Three refinable parameters, namely, $R_{Bragg}$, $R_F$ (*R* structure factor), and $R_P$ (*R* pattern), where the first two parameters deal with only the Bragg peaks, whereas the third one accounts for the background pattern and Bragg peaks, are used. The observed, calculated, and difference X-ray diffraction patterns of 7.5 atom

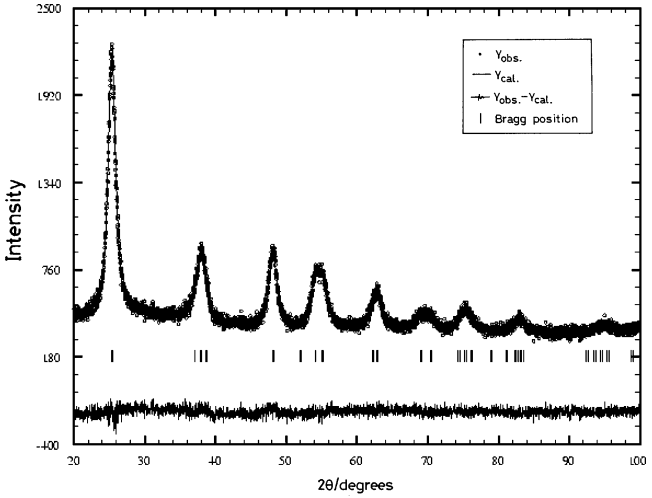


**Figure 2.** Observed (o), calculated (solid line) and difference (bottom) X-ray diffraction pattern of 7.5 atom % $Cu/TiO_2$.

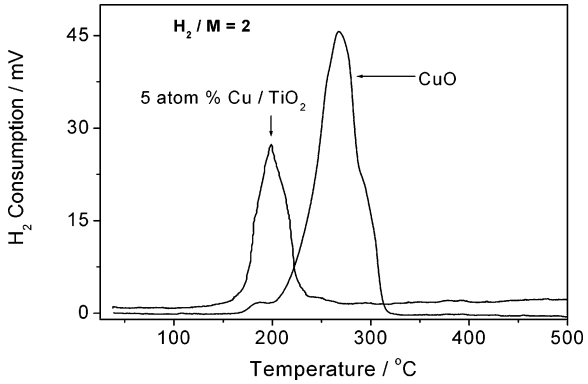


**Figure 3.** Hydrogen uptake of pure CuO and 5 atom % $Cu/TiO_2$.

% $Cu/TiO_2$ are given in Figure 2. A good agreement between the observed and calculated patterns was observed. The $R_{Bragg}$, $R_F$, and $R_P$, values are 3.26, 2.40, and 4.08%, respectively. The lattice parameter $a = 3.782(3)$ Å and $c = 9.481(7)^1$ Å. The fitting is good as seen from $R$ factor values. Pure $TiO_2$ was also refined, and the $R_{Bragg}$, $R_F$, and $R_P$ values of undoped titania are 2.45, 1.53, and 4.87%, respectively. The lattice parameters for pure $TiO_2$ are $a = 3.7904$ (5) Å and $c = 9.5067$ (1) Å. The Debye−Waller factor for the Ti ion indeed decreases from 0.43 to 0.35 from pure $TiO_2$ to $Cu/TiO_2$ indicating an increase in the electron density at the Ti sites in Cu doped titania. Further, $R$ factors increase if the Cu ion is not taken into account in the refinement of $Cu/TiO_2$. The Rietveld refinement indicated $Cu^{2+}$ ion substitution in the combustion synthesized $TiO_2$ matrix. The redox property of the $Cu^{2+}$ ion will be different if the $Cu^{2+}$ ion is substituted in $TiO_2$ compared to that of CuO, which can be examined by temperature programmed reduction (TPR) in hydrogen. Figure 3 shows an TPR profile of 5 atom % $Cu/TiO_2$. The peak reduction temperature of the $Cu^{2+}$ ion in $Cu/TiO_2$ prepared by the solution combustion method is ~ 200 °C, which is lower than that of pure CuO at 270 °C. The volume of hydrogen ($H_2$) used in the reaction is estimated taking CuO as the standard. For CuO, the molar ($H_2$/CuO) ratio was unity for the reaction, $H_2 + CuO \rightarrow Cu + H_2O$. The $H_2$/Cu molar ratio in 5 atom % $Cu/TiO_2$ was 2, which is twice that which is required to reduce $Cu^{2+}$ ions in $Cu/TiO_2$. This cannot be accounted even if we assume that all of the Cu ions are present as CuO. If the $Cu^{2+}$ ion is substituted, part of the $Ti^{4+}$ ions can be reduced to the lower valent Ti ion along with $Cu^{2+}$ to $Cu^0$.

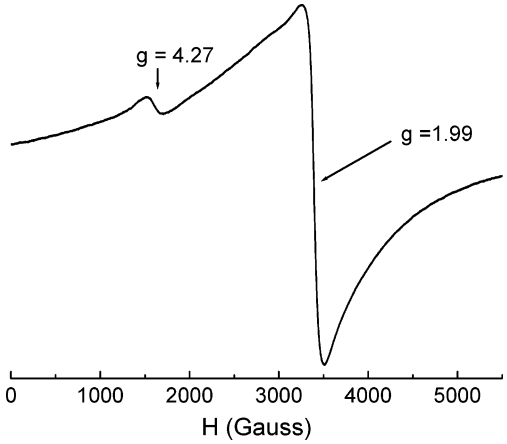


**Figure 4.** EPR spectrum of 5% $Fe/TiO_2$.

**TABLE 1: Rietveld Refinement Parameter of Metal Doped $TiO_2$**

| compound | $R_{Bragg}$ | $R_F$ | $R_P$ | $a$ (Å) | $c$ (Å) |
|---|---|---|---|---|---|
| $TiO_2$ | 2.45 | 1.53 | 4.87 | 3.7904(6) | 9.506(2) |
| $Ti_{0.925}Cu_{0.075}O_{2-\delta}$ | 3.26 | 2.40 | 4.08 | 3.781(3) | 9.481(7) |
| $Ti_{0.925}Fe_{0.075}O_{2-\delta}$ | 7.36 | 5.18 | 10.8 | 3.786(6) | 9.491(5) |
| $Ti_{0.925}Zr_{0.075}O_{2-\delta}$ | 3.62 | 2.71 | 8.5 | 3.7901(4) | 9.544(2) |
| $Ti_{0.975}Ce_{0.025}O_2$ | 4.95 | 4.44 | 11.8 | 3.801(1) | 9.538(3) |
| $Ti_{0.99}W_{0.01}O_{2+\delta}$ | 4.8 | 3.48 | 9.6 | 3.782(4) | 9.493(1) |
| $Ti_{0.95}V_{0.05}O_{2+\delta}$ | 4.71 | 3.34 | 9.42 | 3.792(3) | 9.512(3) |

The XRD, Rietveld refinement and TPR studies suggest that $Cu^{2+}$ is substituted in $Ti^{4+}$ at least up to 7.5%.

*$Ti_{1-x}Fe_xO_{2-\delta}$.* Although Fe doped $TiO_2$ does not show any $Fe_2O_3$ peaks even at 10 atom percent, a small rutile peak is observed at concentrations higher than 5 atom %. $Fe^{3+}$ ion substitution is confirmed by Rietveld analysis. The structural parameters are given in Table 1. Further, the EPR spectrum of iron doped $TiO_2$ shows two signals at $g = 4.27$ and 1.99 (Figure 4). These two signals can be attributed to $Fe^{3+}$ substituted for $Ti^{4+}$ in the $TiO_2$ lattice ($g = 1.99$) and to $Fe^{3+}$ substituted in the lattice adjacent to a charge-compensating oxide anion vacancy ($g = 4.29$) similar to those described by other investigators.[28,29]

*$Ti_{1-x}M_xO_2$ ($M$ = Ce, Zr).* $Ce^{4+}$ ion substitution could be carried out to the extent of 2.5 atom % in $TiO_2$ anatase phase. Even at 5 atom %, diffraction peaks due to $CeO_2$ are observed. However, up to 20 atom %, the $Zr^{4+}$ ion could be substituted for $Ti^{4+}$ in $TiO_2$ anatase phase. Structures of $Ti_{0.975}Ce_{0.025}O_2$ and $Ti_{0.925}Zr_{0.075}O_2$ have been refined and structural parameters are summarized in Table 1. A slight increase in lattice parameters is observed as expected because the ionic radii of $Ce^{4+}$(0.82Å) and Zr $^{4+}$(0.72Å) are higher that $Ti^{4+}$ (0.605).

*$Ti_{1-x}M_xO_{2+\delta}$ ($M$= W, V).* A solid solution with $W^{6+}$ ion could be made for very low concentration, 0.5−1 atom % W. Even at 2 atom %, tungsten doped samples give separate diffraction peaks due to $WO_3$. The mean crystallite sizes of the W doped titania increase with the increase in metal content compared to pure $TiO_2$ indicating W ion substitution. Since the ionic radius of the $W^{6+}$ (0.60 Å) ion is very close to that for the $Ti^{4+}$ (0.605 Å) ion, a $Ti_{1-x}W_xO_2$ solid solution is expected to form at higher W ion concentration. However, doping of $W^{6+}$ in the $Ti^{4+}$ octahedral cationic site leads to the cation vacancy, one $Ti^{4+}$ for every two W ions (expected from the higher ionic charge). Accommodation of excess oxygen or cation vacancy does not seems to be favorable in the $TiO_2$ anatase structure, and hence, $WO_3$ separates out. Similarly, only up to 2.5 atom %, the $V^{5+}$ ion can be substituted in $TiO_2$ anatase structure. An intense rutile

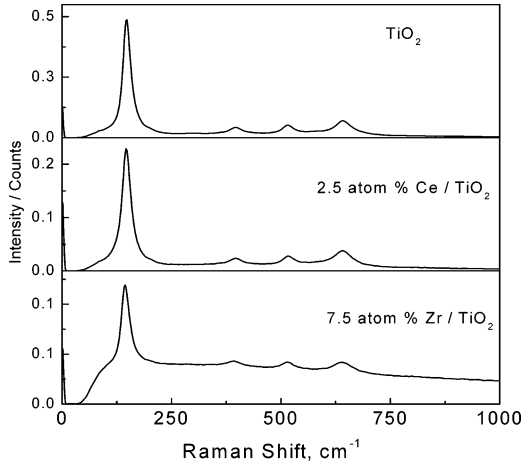


**Figure 5.** Raman spectra of $TiO_2$, 2.5 atom % $Ce/TiO_2$, 7.5 atom % $Zr/TiO_2$.

peak was observed for 5 atom % $V/TiO_2$. Only a small change in the lattice parameters is seen as expected (Table 1).

Thus, structural refinements show that only up to 7.5 atom % $Cu^{2+}$, and 2.5 atom % $Ce^{4+}$, 1 atom % $W^{6+}$ ions could be substituted for $Ti^{4+}$ ion in anatase phase. Though $Fe^{3+}$ and $V^{5+}$ ions can be substituted for $Ti^{4+}$ ion, both the substitution show small rutile impurity. Only $Zr^{4+}$ could be substituted up to 20 atom %. These studies indicate that the solid solution formation of $TiO_2$ with transition metal ions is restricted to a very narrow range of dopant ion concentrations.

**Thermal Stability of Solid Solutions.** To find the stability of metal doped titania, samples were heated at different temperatures for 24 h. At 500 °C, only 3.5% CuO has separated from 5 atom % $Cu/TiO_2$, as seen from the relative intensities of CuO and solid solution diffraction peaks. Heat treatment of the Fe doped $TiO_2$ at 500 °C for 24 h showed diffraction lines due to $Fe_2TiO_5$ oxide phase along with anatase and small rutile phase. It has been found that Cu and Fe dopant ions accelerate the anatase−rutile phase transition. $ZrO_2$ peaks were not observed on heat treatment at 650 °C for 24 h. At 650 °C, pure $TiO_2$ shows an intense rutile peak, whereas both $Ce^{4+}$ and $Zr^{4+}$ substituted $TiO_2$ stabilize anatase phase, prevent phase transformation. The complete transformation of vanadium doped samples to rutile occurs by heat treatment at 600 °C, whereas less than 5% transformation is obtained for the undoped sample treated in an identical condition. Vanadium is known to catalyze phase transformation from anatase to rutile.[30] Thus, stability of solid solution decreases with long time heating. This also suggest that the preparation methods involving long time heating process give lesser amount of metal ion substituted $TiO_2$ compared to solution combustion method.

**Raman Studies.** Raman spectra of metal doped titania are shown in Figure 5. In general, the Raman spectrum of $TiO_2$ is characterized by a strong band at 144 $cm^{-1}$, three mid intensity bands at 396, 517, and 639 $cm^{-1}$, and a weak band at 196 $cm^{-1}$. These six peaks correspond to the six fundamental vibrational modes of anatase $TiO_2$ with the symmetries of $E_g$, $E_g$, $B_{1g}$, $A_{1g}$, $B_{1g}$, and $E_g$, respectively. Raman spectra of 2.5 atom % cerium and 7.5 atom % zirconium doped titania show a typical spectra of anatase $TiO_2$. According to the literature,[31] six Raman active modes ($A_{1g} + 3E_g + 2B_{1g}$) are expected for *t*-$ZrO_2$ (space group $P4_2/nmc$), whereas for the fluorite structure of $CeO_2$ (space group $Fm3m$), only one mode ($F_{2g}$) is Raman active.[32] No Raman lines due to $CeO_2$ or $ZrO_2$ are observed in the above metal doped samples. These results indicate the solid solution formation in the above samples, which is consistent with the XRD measurements.

**TABLE 2: BET Surface Area of Metal Doped Samples**

| catalyst | BET surface area ($m^2/g$) |
|---|---|
| $TiO_2$ | 240 |
| 1 atom % $W/TiO_2$ | 141 |
| 2 atom % $W/TiO_2$ | 119 |
| 2.5 atom % $V/TiO_2$ | 137 |
| 5 atom % $V/TiO_2$ | 110 |
| 2.5 atom % $Ce/TiO_2$ | 97 |
| 5 atom % $Ce/TiO_2$ | 130 |
| 7.5 atom % $Ce/TiO_2$ | 127 |
| 2.5 atom % $Zr/TiO_2$ | 113 |
| 5 atom % $Zr/TiO_2$ | 133 |
| 7.5 atom % $Zr/TiO_2$ | 146 |
| 2.5 atom % $Fe/TiO_2$ | 68 |
| 5 atom % $Fe/TiO_2$ | 64 |
| 7.5 atom % $Fe/TiO_2$ | 58 |

**TABLE 3: Binding Energies of Dopant Metal Ions**

| compound | | binding energy |
|---|---|---|
| 7.5 atom % $Zr/TiO_2$ | Zr $3d_{5/2}$ | 182.2 |
| | Zr $3d_{3/2}$ | 184.4 |
| 5 atom % $V/TiO_2$ | V $2p_{3/2}$ | 517.0 |
| | V $2p_{1/2}$ | 523.0 |
| 2.5 atom % $Ce/TiO_2$ | $Ce3d_{5/2}$ | 883.3 |
| | $Ce3d_{3/2}$ | 900.1 |
| 2.5 atom % $Fe/TiO_2$ | Fe $2p_{3/2}$ | 711.8 |
| | Fe $2p_{1/2}$ | 722.8 |
| 5 atom % $Cu/TiO_2$ | Cu $2p_{3/2}$ | 934.8 |
| | Cu $2p_{1/2}$ | 954.7 |

**Specific Surface Area Measurements.** The specific surface areas of all of the metal substituted $TiO_2$'s were determined (Table 2), and it was found that incorporation of metal ions leads to a decrease in the specific surface area of $TiO_2$. The decrease of the surface area could be attributed to the increase in mean crystallite sizes of the metal doped samples, as evident from the X-ray patterns of the $W^{6+}$ and $V^{5+}$ doped samples. Moreover, as the metal content is further increased, the specific surface area decreases. The decrease of the surface area with the increase in metal content can be attributed to the separation of the dopant metal oxide species dispersed on the surface. The presence of such oxides on the surface at higher concentrations is confirmed by XRD measurements. Even though Zr doped samples have less surface area compared to the undoped counterpart, the surface area increases with the increase in the metal content. This can be due to the surface solid solution formation that prevents particle growth.

**XPS Studies.** Ti ($2p_{3/2,1/2}$) peaks at 459.0 and 464.8 eV show that Ti is in +4 state in all of the metal doped titania. No significant variation in the binding energy of Ti (2p) was observed upon doping metal ions in any of the metal ion substituted oxides. Core level binding energies of the dopant metal ions indicate that dopant ions are present in their highest oxidation state ($Fe^{3+}$, $Cu^{2+}$, $W^{6+}$, $V^{5+}$ $Zr^{4+}$, and $Ce^{4+}$).[33] Binding energies are summarized in Table 3.

Figure 6 shows the valence band region of pure $TiO_2$ and metal doped $TiO_2$. In pure $TiO_2$, Ti atoms are in the +4 oxidation state and the valence band contains only the $O^{2-}$ (2p) contribution. Accordingly, an increase in electron density occurs at about 3 eV, corresponding to the band gap of $TiO_2$. However, in $Cu/TiO_2$, $Cu^{2+}$ (3d) electrons should lie above the O (2p) band similar to that in CuO. Indeed, appreciable electron density below the fermi level ($E_F$) and above the O (2p) band edge was observed in the valence band of $Cu/TiO_2$. In the case of $Fe/TiO_2$, the $Fe^{3+}$ (3d) band is just above the $O^{2-}$ (2p) band. Thus,

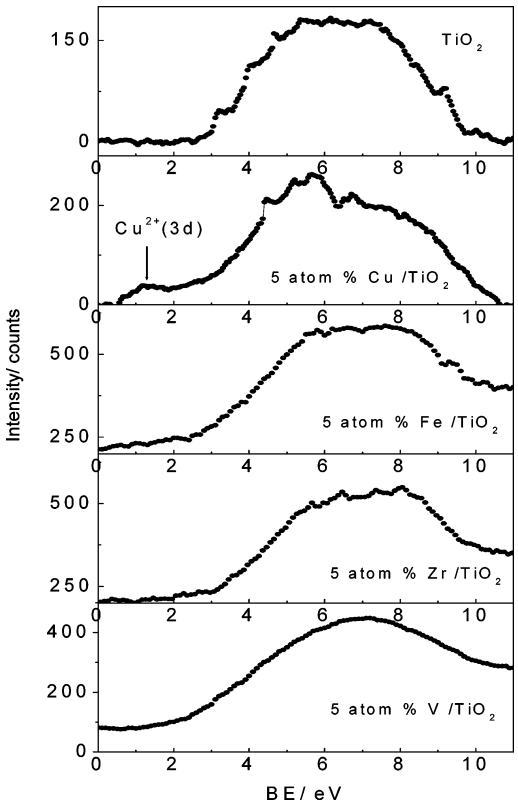


**Figure 6.** Valence band spectra of$TiO_2$ and metal doped $TiO_2$.

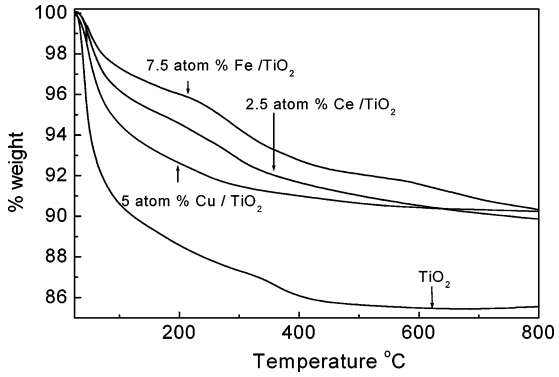


**Figure 7.** TGA of $TiO_2$ and metal doped $TiO_2$.

the Fe (3d) band overlaps with the O (2p) and electron density is observed above the O (2p) band. In the case of $Zr/TiO_2$, Zr atoms are in the 4+ oxidation state and the valence band consists of only the O (2p) band. Since the O (2p) band is stabilized more on Zr doping, there is an increase in the band gap. In the case of $V/TiO_2$, V is in the 5+ oxidation state and the valence band contains only the $O^{2-}$ (2p) contribution.

**Thermal Analysis.** Figure 7 shows thermogravimetry analysis (TGA) of 5 atom % $Cu/TiO_2$ in oxygen (150 $cm^3$/min) at the heating rate of 5 °C/min. The study was carried out with $TiO_2$ for comparison, and the results are given in the same figure. The total weight loss in the whole temperature range is 14.4% for undoped $TiO_2$ and 9.6, 10.2, and 9.5% weight loss for Cu, Ce, and Fe doped titania. There are three regions of weight loss, the first stage is from room temperature to 150 °C, which is caused by the loss of physically adsorbed water. The second stage is from 150 to 500 °C and is due to the removal of strongly bound water or surface hydroxyl groups from the catalyst. The third stage is from 500 to 800 °C, where the mass loss is less than 0.5%. Thermal desorption studies of the combustion synthesized $TiO_2$ from room temperature to 500 °C in a vacuum was carried out, and the results indicate that the primary species to leave the surface of $TiO_2$ is water. Thus the weight loss cannot account for any impurity phase. Thus it is clear that amounts of adsorbed water or surface hydroxyl groups are much higher in undoped $TiO_2$ than that on metal doped titania.

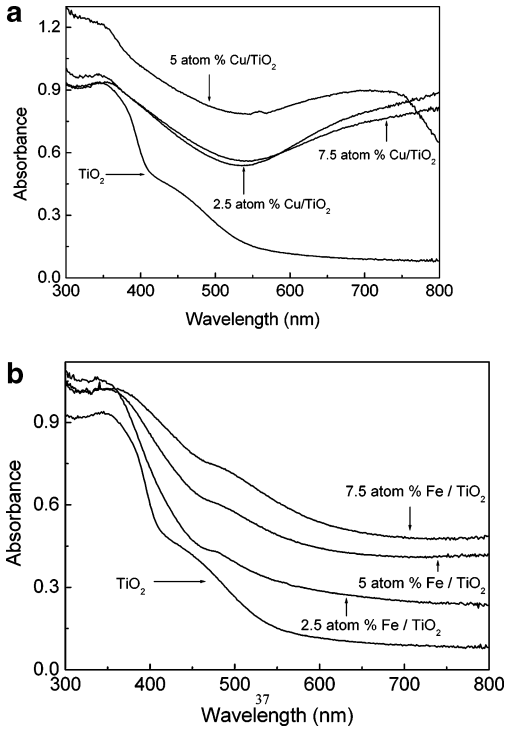


**Figure 8.** UV absorption spectra of (a) Cu doped $TiO_2$ (b) Fe doped $TiO_2$.

**Infrared Studies.** FT-IR spectra of Cu, Fe, and Ce doped $TiO_2$ were compared with that of undoped $TiO_2$. The broad, strong peaks at 3340 and 1625 $cm^{-1}$ show the characteristic absorption of $\delta(-OH)$ stretching and bending mode of the $\delta(-O-H)$ functional group, which is due to Ti−OH and hydrated species. There is a noticeable difference between $TiO_2$ and metal doped $TiO_2$ with a large area reduction for the very large band at 3400 $cm^{-1}$ and for the 1640 $cm^{-1}$ in the case of metal doped $TiO_2$ compared to undoped $TiO_2$. The difference in peak area in the case of metal doped samples demonstrates that metal doped $TiO_2$ powders have less hydroxyl groups in comparison to undoped $TiO_2$ particles. This is consistent with the observation that the surface hydroxyl groups play an important role in the photodegradation process through their interaction with photo generated holes.[34−36]

**Absorption Spectra of Metal Substituted $TiO_2$.** Transition metal doping has a significant effect on absorption characteristics of $TiO_2$. Absorption spectra of Fe and Cu doped $TiO_2$ are presented in Figure 8 and compared to that of the $TiO_2$ prepared by the above method. The combustion synthesized $TiO_2$ shows two optical absorption thresholds at 570 and 467 nm that correspond to the band gap energy of 2.18 and 2.65 eV, respectively. The decrease in the band gap is due to carbide ion substitution for oxide ion in the $TiO_2$ during combustion.[7] Copper doping in titania introduces a band in the visible region at ~800 nm along with the main $TiO_2$ peak at 400 nm. The absorption band at 800 nm is due to the $^2E_g$ to $^2T_{2g}$ transition of the $Cu^{2+}$ ion in the $TiO_2$ matrix. Enhancement of the absorption in the visible region is thus due to the absorption of an isolated $Cu^{2+}$ ion in $TiO_2$. The spectra of Fe doped $TiO_2$ also shows optical absorption in the visible region at 550 and

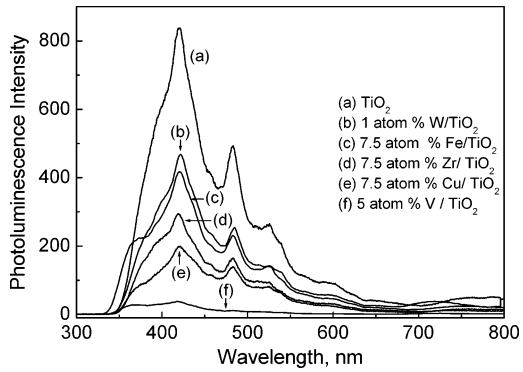


**Figure 9.** Photoluminescence spectra of metal doped $TiO_2$.

400 nm. It is to be noted that the band gap absorption at 400 nm of $TiO_2$ is not affected by Fe doping. The increase in Fe content leads to a linear increase in the absorption band at 550 nm in the visible region. The $Fe^{3+}$ $t_{2g}$ level is close to the VB of $TiO_2$; hence, optical transition is expected to occur from Fe $t_{2g}$ to the CB.

In the case of Zr doped samples, the UV absorption shifts to the lower wavelength region and the blue shift increases with the increase in the metal content. This is due to the large band gap of pure $ZrO_2$ (~5 eV). The W doping has very little effect on the absorption and the optical absorption of W doped samples was similar to $TiO_2$. The optical absorption edge shifts toward higher wavelength in $Ce^{4+}$ doped titania samples. This drop in band gap width may be caused by the formation of continuous shallow impurity levels (Ce 4f levels) in the $TiO_2$ forbidden band after Ce doping. The spectrum of $V^{5+}$doped $TiO_2$, shows enhanced absorption over the entire visible region. This absorption is attributed to the charge transfer between valence band (VB) to the $t_{2g}$ level of vanadium, which lies just below the conduction band.

The origin of the visible spectra in the case of the metal doped sample is due to the formation of a dopant energy level within the band gap of $TiO_2$. The electronic transitions from the valence band to dopant level or from the dopant level to the conduction band can effectively red shift the band edge absorption threshold. Dopants such as $Cu^{2+}$ and $Fe^{3+}$ show d−d transition in the visible region. Thus, optical absorption of metal doped systems depends on the energy levels of the dopants within the $TiO_2$ lattice, their d electronic configuration, and the distribution of the dopants metal ions.[19]

**Photoluminescence of Metal Doped $TiO_2$.** The photoluminescence technique has been widely used in the field of photocatalysis over solid semiconductors as a useful probe for understanding the surface processes in which photo formed electrons and holes take part, i.e., primary processes in photocatalysis. Figure 9 shows photoluminescence (PL) emission spectra of all metal doped titania along with pure $TiO_2$. Luminescence spectra of $TiO_2$ exhibit two emission peaks at 419 and 483 nm with excitation at 285 nm. The emission band at 419 nm is due to free exciton emission of $TiO_2$. The emission band at 483 is due to the surface state such as $Ti^{4+}$−OH. The metal doped $TiO_2$ also shows emission spectra at the same energy as that of pure $TiO_2$. Although the peak positions in the PL of the metal doped titania are in agreement with pure $TiO_2$, the PL intensities are quite sensitive to metal doping. The PL intensities of metal doped titania are much lower than that of the undoped titania. The quenching increases with the increase in the amount of doping (see the Supporting Information, Figure S1). This is attributed to the enhanced metal−metal interaction at higher concentrations.[37]

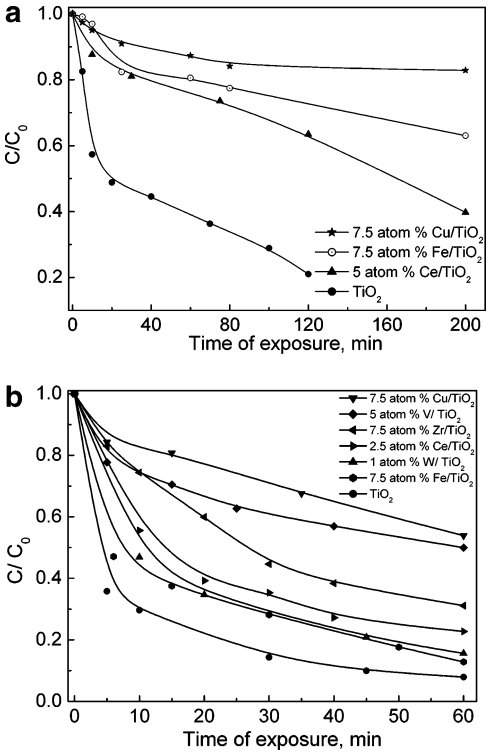


**Figure 10.** Degradation profiles of 4-nitrophenol of 0.5 mM initial concentration with catalyst loading of 1 kg/m$^3$ over metal doped $TiO_2$ and combustion synthesized $TiO_2$ (a) solar (b) UV exposure.

Since excitation was carried out under equal absorption conditions at 285 nm, the decrease in emission intensities must originate from the differences in electronic structure of the metal doped samples. The observed decrease in the photoluminescence intensity on metal doping can be attributed to the electron transfer processes from the excited state (CB) to the new levels introduced by the metal dopants. The free hole can recombine with a trapped electron, or a free electron can recombine with a trapped hole. These recombination processes can be nonradiative and quench the fluorescence. If it is radiative, the emission energy can be considerably less than $E_g$, and emission can occur at higher wavelength.

The decrease in emission intensity can also be due to the introduction of new defect sites such as oxide ion vacancy. Oxygen vacancy can trap an electron in the following pathway:[38]

$$V_O^0 + e_{CB}^- \rightarrow V_O \quad \text{(Electron trapping in shallow traps)} \quad (1)$$

$$V_O + h_{VB}^+ \rightarrow V_O^0 + h\nu \quad \text{(Radiative recombination)} \quad (2)$$

The ionized oxygen vacancy level is poised to rapidly trap a photogenerated CB electron that subsequently interacts with a valence band hole either radiatively or nonradiatively.

**Photocatalytic Activity of Metal Doped $TiO_2$.** Degradation of 4-nitrophenol is not significant in the absence of $TiO_2$ and no degradation occurs in the absence of light when $TiO_2$ is present. Figure 10a shows the degradation profile of 4-nitrophenol under solar irradiation with an initial concentration of 0.5 mM (69.5 ppm) and the catalyst loading of 1 kg m$^{-3}$. An 80% decrease in the concentration of 4-nitrophenol is observed in 120 min in the presence of pure $TiO_2$. Only 16.5%, 26%, and 36% decreases in concentration are observed at 120 min with 5 atom % Cu doped $TiO_2$, 7.5 atom % Fe/$TiO_2$, and 2.5 atom % Ce/$TiO_2$. Although the metal doped titania absorbs in

the visible region, the visible light photoactivity is lower than undoped titania prepared by this method.

On metal doping, the activity of $TiO_2$ in the presence of UV also decreased. Figure 10b shows the degradation of 4-nitrophenol catalyzed by metal doped $TiO_2$ under UV exposure as a function of irradiance time. The complete degradation of nitrophenol was observed with $TiO_2$, whereas ionically substituted transition metals for $Ti^{4+}$ in $TiO_2$ decrease the activity of $TiO_2$. The comparison of photocatalytic activities of undoped $TiO_2$ and highest metal content doped compounds show activity in this order: $TiO_2 > Fe/TiO_2 > W/TiO_2 > Ce/TiO_2 > Zr/TiO_2 > V/TiO_2 \sim Cu/TiO_2$. The photocatalytic activity of 2.5, 5, and 7.5 atom % $Cu/TiO_2$ on the degradation of 4-nitrophenol was measured (Supporting Information, Figure S2). As the copper content increases, the degradation rate decreases, which indeed correlates with the photoluminescence of the material (Supporting Information, Figure S1). Experiments were also carried out (not shown) with 0.5, 1, and 2 atom % $Cu/TiO_2$ and the photocatalytic activity reduced with increasing copper content. At even lower amounts of metal species, the effect on the photocatalytic activity was not significant. The objective of this study was to find if metal ion substitution influences the photocatalytic activity. Because the maximum effect can be observed only at high concentrations of metal ions, we have shown the results for the highest substituted metal ions in each case. Unequivocal assertion of the effect of substitution at very low metal ion substitution is difficult because the photocatalytic activity of these materials would be similar to that of $TiO_2$. To test if CuO has any negative effect on the photocatalytic activity, an experiment was carried out with a physical mixture of 7.5 atom % CuO + $TiO_2$ and the activity was compared with combustion synthesized $TiO_2$ and 7.5 at. % $Cu/TiO_2$ (see the Supporting Information, Figure S3). The physical mixture of 7.5 atom % CuO +$TiO_2$ shows a complete degradation, and the activity is comparable to that of pure $TiO_2$, whereas 7.5 atom % Cu doped titania shows only 40% decrease in concentration under identical condition. Therefore, the detrimental effect is due to $Cu^{2+}$ ion substitution to the $Ti^{4+}$ in $TiO_2$. Even though $WO_3$ is a known photocatalyst with band gap of 2.8 eV, doping of W in titania did not enhance the photoactivity of $TiO_2$. In the case of Ce doped titania, 2.5 atom % Ce doped $TiO_2$ shows the least activity, and the activity was relatively higher with 5 and 7.5 atom %. Possible explanations are that combustion synthesized $CeO_2$ itself shows complete degradation of 4-nitrophenol. The separation of $CeO_2$ particles could be the reason for higher activity of 5 and 7.5 atom % Ce doped samples compared to 2.5 atom % $Ce/TiO_2$. Although Fe doping shows a decrease in photocatalytic activity, its effect was smaller than the extent of decrease of photocatalytic activity with other metal doped systems. However, the photocatalytic activity of most of metal doped $TiO_2$ is higher than the photocatalytic activity of Degussa P25 $TiO_2$ catalyst (see Figure 11).

In an earlier study, photocatalytic reaction was carried out on 1 atom % Pt metal impregnated on $TiO_2$ and compared with the Pt metal ion substituted $TiO_2$ and undoped $TiO_2$. The results show that the impregnated $Pt^0$ has a higher activity than the Pt ions substituted $TiO_2$ and $TiO_2$ alone.[25] However, UV absorption spectrum of platinum impregnated samples show neither an increase of absorption in the UV region nor a shift in the band gap on platinisation. Therefore, an enhancement of the photoactivity by these effects must be excluded. Deposits of platinum enhance the separation of the electron- hole pairs in a semiconductor. Platinum metal islands are very effective traps for the electrons due to the formation of a Schottky barrier at the metal-semiconductor contact,[2] whereas ionically substituted Pt metal for Ti $^{4+}$ in $TiO_2$ creates new energy levels and act as charge carrier recombination center.

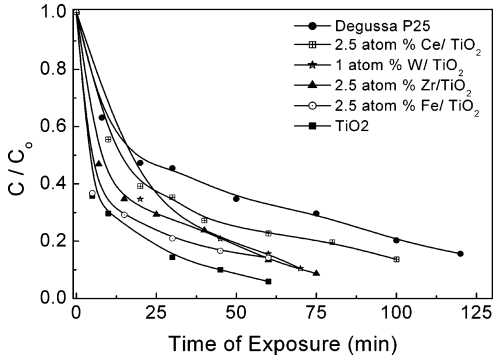


**Figure 11.** Degradation profiles of 4-nitrophenol over metal doped $TiO_2$ and Degussa P25.

## Discussion

XRD and Raman studies of doped samples prepared by the solution combustion method showed no significant variations in the size, crystallinity, and crystal structure of the doped samples compared with the undoped titania. The solid solution formation of metal ions with $TiO_2$ is restricted to a very narrow range of doped ion concentrations. Though the specific surface area of metal substituted $TiO_2$ was lower than the undoped titania, the photo activity is not a mere function of surface area as we have seen earlier.[26] The lesser amount of surface hydroxyl groups was observed in case of metal doped $TiO_2$ compared to the undoped $TiO_2$. This could be one of the reasons for the lower activity of metal doped $TiO_2$.

Most of the metal doped $TiO_2$ absorbs in the visible region. However, the photocatalytic activity of metal doped $TiO_2$ demonstrated that there is no direct correlation between the light absorption capacity of the metal doped catalyst and the rate of degradation. It should be noted that under UV exposure, also, degradation rates were in general less than the undoped $TiO_2$. During the photocatalytic process, the absorption of photons by the photocatalyst leads to the excitation of electrons from the valence band to the conduction band, thus generating electron−hole pairs. The electron in the conduction band is captured by oxygen molecules dissolved in the suspension, and the hole in the valence band can be captured by $OH^-$ or $H_2O$ species adsorbed on the surface of the catalyst, to produce the hydroxyl radical. These hydroxyl radicals then oxidize the pollutants. Thus, recombination of photogenerated electrons and holes is one of the most significant factors that determine the photoactivity of the $TiO_2$. Any factor that suppresses the electron hole recombination will therefore enhance the photocatalytic activity.

The presence of metal ions in titania does not modify the position of the valence band edge of anatase as seen from photoluminescence. Instead, it introduces new energy levels of the transition metal ions into the band gap of $TiO_2$.[19] From X-ray photoelectron spectroscopy of metal doped $TiO_2$ and corresponding oxides, relative positions of metal (d and f) and O (2p) levels can be obtained. The $Cu^{2+}$ (3d) band is clearly observed at ∼1−2 eV below fermi level ($E_F$) in $Cu/TiO_2$. In the case of $Fe/TiO_2$, the $Fe^{3+}$ (3d) band is just above the $O^{2-}$ (2p) band as has been seen in $Fe_2O_3$.[39] In the XPS of $Fe/TiO_2$, the Fe (3d) band is not seen separately. In the case of $ZrO_2$, the O (2p) band is stabilized more than in $TiO_2$, and hence, there is an increase in the band gap. Ce ($4f^0$) is located at about 1.5

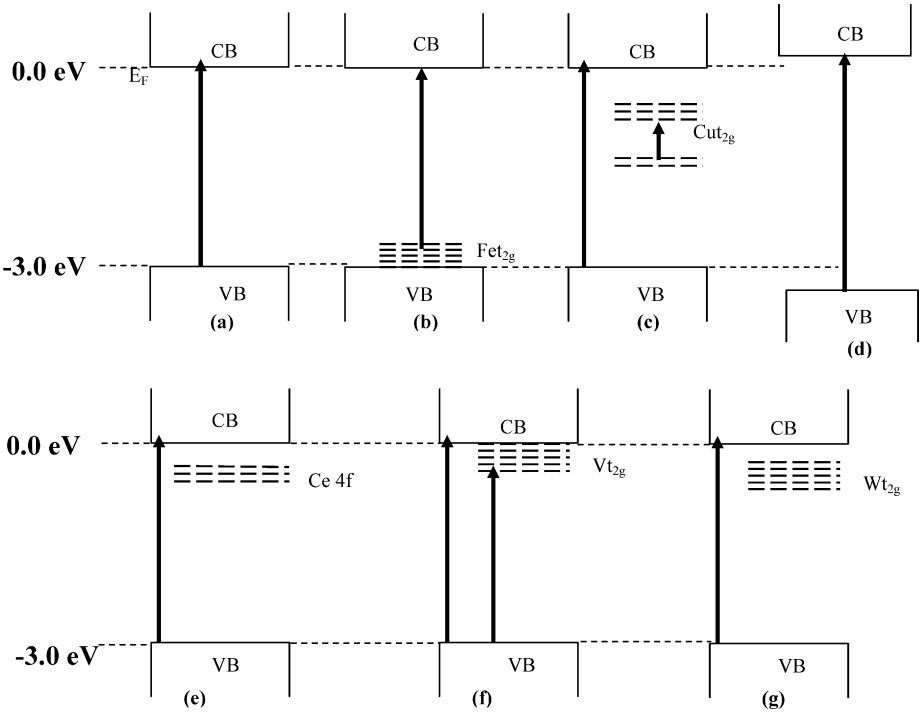


**Figure 12.** Schematic representation of energy levels of dopant ions in $TiO_2$, (a) $TiO_2$, (b) $Fe/TiO_2$, (c) $Cu/TiO_2$, (d) $Zr/TiO_2$, (e) $Ce/TiO_2$, (f) $V/TiO_2$, and (g) $W/TiO_2$.

eV below the CB edge.[40] The $V^{5+}$ (3d) bands also lie below the CB edge of $TiO_2$. V (3d) bands in $VO_2$ and $V_2O_3$ are indeed below the Fermi level ($E_F$), well separated from O (2p).[41] Accordingly, energy level diagram of metal doped $TiO_2$ is shown in Figure 12. This energy level diagram is similar to those reported by Mizushima et al.[42,43] This is to be correlated with the corresponding decease in photoluminescence.

The energy levels created due to metal ion doping in $TiO_2$ act as $e^-/h^+$ trapping centers as seen from photoluminescence measurements. When the energy levels of the metal ion impurities lie below the conduction band edge, it traps the excited electrons. When the energy level is above the valence band edge, electrons in the d orbitals can quench the photogenerated holes by indirect recombination before they can diffuse to the surface. The electron trapping is a much faster process ($\tau \sim 30$ ps) than the hole trapping ($\tau \sim 250$ ns)[19] (eqs 3−6).

$$TiO_2 + h\nu \rightarrow h^+_{VB} + e^-_{CB},\ \tau = 10^{-15}\ s \quad (3)$$

$$e^-_{tr} + h^+_{tr} \rightarrow \text{heat},\ \tau = 10^{-9}\ s \quad (4)$$

$$e^-_{CB} \rightarrow e^-_{tr}\,(M^{n+}/O_2),\ \tau \sim 30\ ps \quad (5)$$

$$h^+_{VB} \rightarrow h^+_{tr}\,(OH^-/M^{(n+1)}),\ \tau \sim 250\ ns \quad (6)$$

The presence of metal ion dopants provides more trap sites for electrons and holes in addition to the surface trap sites (adsorbed $O_2$ and $-OH^-$). Trapping either an electron or a hole alone is ineffective for photodegradation because immobilized charge species quickly recombines with its mobile counterpart.[19] This recombination process is faster than $h^+$ trapping by the hydroxyl species itself (eqs 7−8).

$$e^-_{tr} + h^+_{VB} \rightarrow TiO_2,\ \tau \sim 30\ ns \quad (7)$$

$$e^-_{tr} + h^+_{tr} \rightarrow TiO_2,\ \text{slow} \quad (8)$$

Thus, substituted metal ions act as recombination centers instead of suppressing electron hole recombination. Transition metal ions doping influences the photoactivity detrimentally because it increases the recombination rate of hole/electron pairs as confirmed from the photoluminescence studies, whereas metal particles deposited on $TiO_2$ enhance the photocatalytic activity because they enhance the separation of the electron hole pairs in the semiconductor. Platinum metal island are very effective traps for the electrons. Thus, they prevent electron hole recombination. However, $Pt^{2+}$ ion substituted $TiO_2$ is ineffective for photocatalysis because $Pt^{2+}$ (d) states lying below CB act as traps. Different behavior of various metal doped $TiO_2$ can be related to the solubility of the transition metal ion in $TiO_2$ and the position of metal d levels with in the band gap energy of $TiO_2$. Therefore, transition metal ions substituted for $Ti^{4+}$ in $TiO_2$ do not enhance photocatalytic activity even with an extension of absorption in the visible region.

**Acknowledgment.** Financial support from the Department of Science and Technology, Government of India is gratefully acknowledged.

**Supporting Information Available:** Photoluminescence spectra of Cu doped $TiO_2$ (Figure S1); Degradation profiles of 4-nitrophenol over Cu doped $TiO_2$ (Figure S2); Degradation profiles of 4-nitrophenol over CuO + $TiO_2$ (Figure S3). This material is available free of charge via the Internet at http://pubs.acs.org.

## References and Notes

(1) Hoffmann, M. R.; Martin, S. T.; Choi, W.; Bahnemann, D. W. *Chem. Rev.* **1995**, *95*, 69.
(2) Linsebrigler, A. L.; Lu, G.; Yates, J. T. *Chem. Rev.* **1995**, *95*, 735.
(3) Fujishima, A.; Rao, T. N.; Tryk, D. A. *J. Photochem. Photobiol. C: Photochem. Rev.* **2000**, *1*, 1.
(4) Ollis, D. F.; Al-Ekabi, H. *Photocatalytic Purification and treatment of Water and Air*; Elsevier: Amsterdam, 1993.
(5) Asahi, R.; Morikawa, T.; Ohwaki, T.; AoKi, K.; Taga, Y. *Science* **2001**, *293*, 269.
(6) Khan, S. U. M.; Al-Shahry, M.; Ingler, Jr., W. B. *Science* **2002**, *297*, 2243.

(7) Nagaveni, K.; Hegde, M. S.; Ravishankar, N.; Subbanna, G. N.; Madras. G. *Langmuir* **2004**, *20*, 2900.
(8) Butler, E. C.; Davis, A. P. *J. Photochem. Photobiol. A: Chem.* **1993**, *70*, 273.
(9) Di Paola, A.; Lopez, E. G.; Ikeda, S.; Marci, G.; Ohatani, B.; Palmisano, L. *Catal. Today*. **2002**, *75*, 87.
(10) Yu, J. C.; Lin, J.; Kwok, R. W. M. *J. Phys. Chem*. **1998**, *102*, 5094.
(11) Fuerte, A.; Hernández-Alonso, M. D.; Maira, A. J.; Martìnez-Arias, A.; Fernández-García, M.; Conesa, J. C.; Soria, J.; Munuera, G. *J. Catal.* **2002**, *212*, 1.
(12) Serpone, N.; Lawless, D. *Langmuir* **1994**, *10*, 643.
(13) Sclafani, A.; Palmisano, L.; Davi, E. *J. Photochem. Photobiol. A: Chem.* **1991**, *53*, 113.
(14) Grzybowska, B.; Słoczynski, J.; Grabowski, R.; Samson, K.; Gressel, I.; Wcisło, K.; Gengembre, L.; Barbaux, Y. *Appl. Catal. A: Gen.* **2002**, *230*, 1.
(15) Yu, J. C.; Lin, J.; Kwok, R. W. M. *J. Photochem. Photobiol. A: Chem.* **1997**, *111*, 199.
(16) Borgarello, E.; Kiwi, J.; Grätzel, M.; Pelizzetti, E.; Visca, M. *J. Am. Chem. Soc*. **1982**, *104*, 2996.
(17) Lin, J.; Yu, J. C.; Lo, D.; Lam, S. K. *J. Catal.* **1999**, *183*, 368.
(18) Karakitsou, K. E.; Verykios, X. E. *J. Phys. Chem.* **1993**, *97*, 1184.
(19) Choi, W.; Termin, A.; Hoffmann, M. R. *J. Phys. Chem.* **1994**, *98*, 13669.
(20) Palmisano, L.; Augugliaro, V.; Sclafani, A.; Schiavello, M. *J. Phys. Chem*. **1988**, *92*, 6710.
(21) Luo, Z.; Gao, Q.-H. *J. Photochem. Photobiol. A: Chem*. **1992**, *63*, 367.
(22) Priolkar, K. R.; Bera, P.; Sarode, P. R.; Hegde, M. S.; Emura, S.; Kumashiro, R.; Lalla, N. P. *Chem. Mater*. **2002**, *14*, 2120.
(23) Bera, P.; Priolkar, K. R.; Sarode, P. R.; Hegde, M. S.; Emura, S.; Kumashiro, R.; Lalla, N. P. *Chem. Mater*. **2002**, *14*, 3591.
(24) Bera, P.; Gayen, A.; Hegde, M. S.; Lalla, N. P.; Spadaro, L.; Frusteri, F.; Aruna, F. *J. Phys. Chem. B* **2003**, *107*, 6122.
(25) Sivalingam, G.; Nagaveni, K.; Hegde, M. S.; Madras, G. *Appl. Catal. B: Environ*. **2003**, *45*, 23.
(26) Nagaveni, K.; Sivalingam, G.; Hegde, M. S.; Madras, G. *Appl. Catal. B: Environ.* **2004**, *48*, 83.
(27) Nagaveni, K.; Sivalingam, G.; Hegde, M. S.; and Madras, G. *Environ. Sci. Technol*. **2004**, *38* (5), 1600.
(28) Grätzel, M.; Howe, R. F. *J. Phys. Chem.* **1990**, *94*, 2566.
(29) Bickley, R. I.; Lees, J. S.; Tilley, R. J. D.; Palmisano, L.; Schiavello, M. *J. Chem. Soc., Faraday Trans.* **1992**, *88*, 377.
(30) Martin, S. T.; Morrison, C. L.; Hoffmann, M. R. *J. Phys. Chem*. **1983**, *98*, 13695.
(31) Yashima, M.; Arashi, H.; Kakihana, M.; Yoshimura, M. *J. Am. Ceram. Soc*. **1994**, *77*, 1067.
(32) Martinez-Arias, A.; Fernandez-Garcia, M.; Salamanca, L. N.; Valenzuela, R. X.; Oria, J. C. *J. Phys. Chem. B* **2000**, *104*, 4038.
(33) Briggs, D.; Seah, M. P. *Practical Surface Analysis by Auger and X-ray Photoelectron Spectroscopy*; John Wiley & Sons: New York, 1984.
(34) Turchi, C. S.; Ollis, D. F. *J. Catal.* **1990**, *122*, 178.
(35) Sato, S. *Langmuir* **1988**, *4*, 1156.
(36) Bandara, J.; Mielczarski, J. A.; Kiwi, J. *Langmuir*, **1999**, *15*, 7680.
(37) Kang, M. *J. Mol. Catal. A: Chem*. **2003**, *197*, 173.
(38) Sooklal, K.; Cullum, B. S.; Angel, S. M.; Murphy, C. J. *J. Phys. Chem. B* **1996**, *100*, 4551.
(39) Vasudevan, S.; Hegde, M. S.; Rao, C. N. R. *J. Solid State Chem.* **1979**, *29*, 253.
(40) Sharma, D. D.; Hegde, M. S.; Rao, C. N. R. *J. Chem. Soc., Faraday Trans. 2* **1981**, *77*, 1509.
(41) Vasudevan, S.; Hegde, M. S. *Pramana* **1979**, *12*, 151.
(42) Mizushima, K.; Tanaka, M.; Ashi, A.; Iida, S. *J. Phys. Chem. Soilds.* **1979**, *40*, 1129.
(43) Mizushima, K.; Tanaka, M.; Iida, S. *J. Phys. Soc. Jpn.* **1972**, *32*, 1519.